Journal of the Energy Institute 119 (2025) 102008

Contents lists available at ScienceDirect

Journal of the Energy Institute

journal homepage: www.elsevier.com/locate/joei

Investigation on the impact of air equivalence ratio on the characteristics of lignite coal partial gasification products in fluidized bed

Bin Zhang [1], Zhihua Tian [1], Qinhui Wang [*], Dong Ma, Ruiqing Jia

State Key Laboratory of Clean Energy Utilization, Zhejiang University, Hangzhou, 310027, PR China

ARTICLE INFO

Handling editor: Paul Williams

Keywords:
Coal partial gasification
Air equivalence ratio
Product characteristics
Fluidized bed
Gasification index

ABSTRACT

To promote the efficient and clean utilization of inferior coals such as lignite, this study investigated the impact of air equivalence ratios (ER) on the partial gasification performance and product characteristics of lignite in a self-constructed fluidized bed reactor. The three-phase products of char, syngas and tar were characterized using GC-MS, FTIR, Raman, BET and TG. Results indicated that as ER increased from 0.06 to 0.14, the reaction of Shaerhu coal (SC) transitioned from pyrolysis to gasification. The percentage content of combustible gas components (CGC) in the syngas initially increased and then decreased, while the CGC yield continued to rise. Syngas achieved a maximum lower heating value of 2.15 MJ/Nm^3 at an ER of 0.08 and a maximum gasification efficiency of 24.09 % at an ER of 0.14. The yields of char and tar decreased as ER increased. The tar was dominated by phenolic compounds and monocyclic aromatic hydrocarbons and their derivatives, with heavier components ($>C_{20}$) shifting towards lighter fractions ($<C_{10}$). Char combustion characteristics decreased gradually with increasing ER. As ER increased from 0.06 to 0.1, the content of oxygen-containing functional groups in char increased to its peak and the char structure became most disordered. When ER exceeded 0.1, these functional groups were consumed, leading to a more ordered char structure.

1. Introduction

Coal continues to be the most significant non-renewable energy source in the world [1] currently and is essential to the energy structure of China [2]. Coal is a fossil fuel that is challenging to use cleanly and extensive use of it has seriously contaminated the environment [3]. Although China has abundant coal resources, low-quality low-rank coal, which includes lignite coal, accounts for 55.1 % of the total proven coal reserves [4]. Both efficient and clean use of lignite resources has become a major concern as a result of the increased focus on the development and clean use of lignite in recent years [5].

Coal gasification is an effective method for the clean and high-resource utilization of coal [6]. The coal gasification process is typically divided into two stages [7,8]: pyrolysis and char gasification. Traditional gasification processes inevitably waste high-value components of coal [9] and necessitate a continuous external heat source and high-purity oxygen, leading to high costs. The oxidant is used in coal partial gasification to partially gasify the coal [10,11], turning the more reactive parts into coal gas and tar while burning the less reactive char to generate electricity [12]. This method does not aim for an excessively high carbon conversion rate and has lower requirements for reaction temperature and pressure. Additionally, since gasification is a highly exothermic process, it eliminates the need for a continuous external heat source which reduces costs [13]. Consequently, coal partial gasification technology presents a feasible approach for the efficient and clean utilization of lignite resources.

Scholars have conducted extensive research on coal partial gasification. They primarily focus on the production of high-value products, such as syngas with high hydrogen or methanol content [12,14], and the effects of different reaction conditions [15] (e.g., temperature, gasification agent) on the characteristics of partial gasification products. Ye et al. [12] proposed a methanol-electricity cogeneration system based on partial gasification, with experimental results demonstrating the promising application prospects of the system. Zhang [10] and Tokmurzin [16] also discovered that there were greater financial and ecological advantages when coal partial gasification technology was used to construct a coal gasification integrated power generation system. By investigating the migration and alteration of sulfur and nitrogen

* Corresponding author.
E-mail address: qhwang@zju.edu.cn (Q. Wang).
[1] These authors contributed equally to this work.

https://doi.org/10.1016/j.joei.2025.102008
Received 9 September 2024; Received in revised form 16 January 2025; Accepted 21 January 2025
Available online 27 January 2025

elements during partial gasification, Middleton et al. [17] identified the distribution of coal quality, coal nitrogen, and coal sulfur between char and gas. Zhang et al.[18,19] performed partial coal gasification in a steam atmosphere, producing hydrogen-rich syngas and porous carbon with the addition of a K_2CO_3 catalyst. Zhou et al. [11] found that the ratio of gasifying agent to coal during partial gasification significantly influenced the properties of the product syngas. Ye et al.[20,21] conducted partial coal gasification experiments in CO_2/O_2 and H_2O/O_2 atmospheres. The results showed experiments conducted in a CO_2 atmosphere enlarged the pores of the char, generated new oxygen-containing functional groups and increased the number of aromatic rings, resulting in a more disordered structure of char. Conversely, partial gasification in a steam atmosphere made the structure of the char more ordered, leading to a decrease in its reactivity. Song et al. [13] discovered that increasing the equivalence ratio from 0.06 to 0.13 led to a higher partial gasification temperature, a decrease in char yield and an increase in tar yield. Huang et al. [22] found that high-rank bituminous coal had a greater combustible component content in the syngas that resulted from partial gasification than low-rank bituminous coal. Additionally, they noticed that the gasification rate could be greatly accelerated by compounds containing alkali which was consistent with the research results of Wang et al. [23] Zhang et al. [24] studied the influence of the time and proportion of secondary air distribution on NOx emissions and reduced the NO_x emissions during partial gasification. Although scholars had conducted extensive research on coal partial gasification, most of the studies had been carried out at relatively high gasification temperatures exceeding 800 °C. Gasification at high temperatures not only required more external heat sources but also reduced the yield of tar [25] and caused slagging in the furnace. Furthermore, the majority of the coal utilized in the studies is bituminous coal or another type of premium coking coal with little research conducted on low-quality coal such as lignite. Researchers have primarily investigated the changes in product characteristics from the perspective of the gasification atmosphere but gasification is also significantly influenced by the air equivalence ratio. In contrast to gasifiers like CO_2 and H_2O, air is cheap, plentiful and simple to obtain [26]. Therefore, investigating the utilization of air as a gasifier is equally crucial. To enhance the efficient and clean utilization of lignite, experimental research on the products obtained by partial gasification of lignite at different air equivalence ratios is of significant research value.

In this study, we employed air as gasification agents in a self-built fluidized bed to investigate the effects of different air equivalent ratios (ER) on the characteristics of lignite partial gasification products at low temperatures. The obtained syngas, tar, and char were analyzed using GC-MS, FTIR, XRD, BET and TG to determine the optimal ER of partial gasification. Based on the results of these characterization tests, the mechanism by which the ER affects the characteristics of the products was investigated. The findings of this study can offer theoretical direction and a useful foundation to improve the effective and environmentally friendly use of lignite.

2. Materials and methods

2.1. Materials

The coal samples used in this study were Shaerhu coal (SC) from Xinjiang Province, which is a high-volatile lignite. Coal samples with particle sizes of 0.9–2 mm were selected as the experimental raw materials after crushing and sieving. Before the experiment, the coal samples were placed in an oven at 105 °C for 6 h to remove moisture. The proximate and ultimate analyses of the coal samples were conducted by the standards GB/T 212–2008 and GB/T 31,391-2015 with the specific results listed in Table 1. The particle size of the quartz sand used in this study was screened to 0.25–0.45 mm.

2.2. Coal partial gasification experiment

The experiments in this study were conducted using a self-designed bubbling fluidized bed reactor, as illustrated in Fig. 1. The experimental system consists of three main components: a gas system, a reaction system, and a collection and analysis system. The fluidized bed reactor tube is heated using electric heating wires and silicon carbide rods, capable of reaching a maximum temperature of 950 °C, and is insulated with refractory bricks. A preheating section is installed before the fluidized bed to heat the carrier gas to a desired temperature before entering the reactor. After going through a tar condensation device, the gas created during the experiment is collected in an airbag. The collected gas and tar are analyzed by GC1 and GC2, respectively. The char is collected through the hopper at the bottom of the fluidized bed and subsequently characterized. Each set of experiments was averaged three times to remove the effect of error.

To investigate the product characteristics of SC partial gasification at low temperatures, the fluidized bed was heated to 650 °C. For each experiment, 150 g of quartz sand was used as the heat carrier and 10 g of SC was added to the feeder with the feeding rate adjusted to achieve a coal feed rate of 0.289 kg/h. Each reaction lasted for 2 min, corresponding to the time it took for 10 g of coal to fall. To ensure the bed material remained fluidized without being blown out, the airflow and N_2 flow rates were adjusted to maintain a total flow rate of 4.2 L/min. The airflow rate at different air equivalent ratios (ER) was calculated using Eq. (1), with the specific experimental conditions detailed in Table 2.

2.3. Calculation of gasification index

After the experiment, the gasification indexes were calculated based on the analysis results of the products. The calculation methods are as follows.

2.3.1. Air equivalent ratio

The air equivalence ratio (ER) is defined as the ratio of the air supplied under experimental conditions to the air required under stoichiometric conditions. As shown in Eq. (1):

$$ER = \frac{Air_{exp}}{Air_{stoic}} = \frac{V_{air}}{V_{coal}\cdot\left[0.0889\cdot(C_{ad}+0.375S_{ad})+0.265\cdot\left(H_{ad}-\frac{O_{ad}}{8}\right)\right]} \quad (1)$$

where ER represents the air equivalent ratio; V_{coal} (g/min) represents the coal feed rate; V_{air} (L/min) represents the air supply rate.

2.3.2. The yield of partial gasification product

The yields of char, tar and syngas were calculated according to Eqs. (2)–(5):

Table 1
Proximate, ultimate and calorific value analysis of coal.

Sample	Proximate analysis (ad, wt%)				Ultimate analysis (ad, wt%)					LHV (MJ/kg)
	M	A	V	FC	C	H	N	S_t	O_{diff}	
SC	5.04	5.66	43.60	45.70	66.27	5.12	1.01	0.35	16.55	28.33

Note: (1) M: Moisture, A: Ash, V: Volatile, FC: Fixed carbon; (2) ad: Air dry basis, t: Total, diff: By difference.

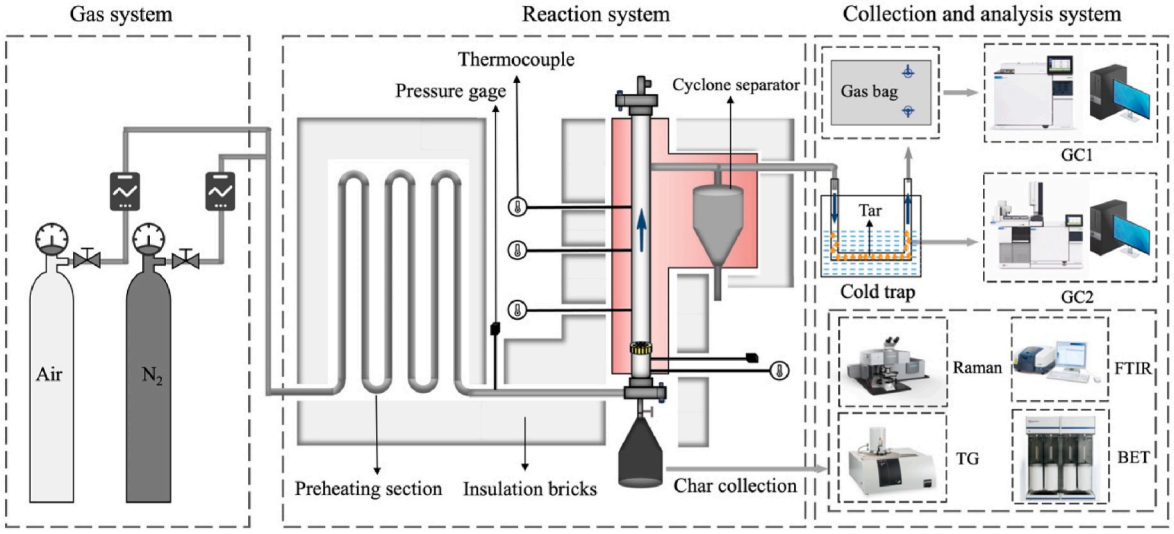

Fig. 1. Schematic diagram of small fluidized bed reactor system.

Table 2
The specific experimental conditions.

Case	ER	Air flow rate (L/min)	N_2 flow rate (L/min)
1	0.06	1.96	2.44
2	0.08	2.57	1.83
3	0.1	3.18	1.12
4	0.12	3.79	0.61
5	0.14	4.4	0

$$Y_{char} = \frac{m_{char}}{m_{coal}} \cdot 100\% \tag{2}$$

$$Y_{liquid} = \frac{m_{liquid}}{m_{coal}} \cdot 100\% = \frac{m_2 - m_1}{m_{coal}} \cdot 100\% \tag{3}$$

$$Y_{tar} = \frac{m_{liquid} - m_{water}}{m_{coal}} \cdot 100\% \tag{4}$$

$$Y_{gas} = \left(1 - Y_{liquid} - Y_{char}\right) \cdot 100\% \tag{5}$$

where Y_{char}, Y_{liquid}, Y_{tar}, Y_{gas} (%) represent the yields of char, liquid products, tar and syngas generated by coal partial gasification, respectively; m_{char}, m_{tar}, m_{liquid}, m_{coal} (g) represent the mass of char, tar, liquid products and coal, respectively; m_2 and m_1 (g) represent the mass of the tar condensation unit after and before the reaction.

2.3.3. Syngas lower heating value and gasification efficiency

The lower heating value (LHV) of syngas was calculated according to Eq. (6):

$$LHV_{gas} = \sum V_i LHV_i \tag{6}$$

where LHV_{gas} (MJ/Nm^3) represents the lower heating value of syngas; V_i (%) represents the volume fraction of various combustible gases in syngas; LHV_i represents the lower heating value of various combustible gases, as shown in Table 3.

The gasification efficiency is defined as the ratio of the chemical energy of the syngas produced by the gasification reaction to the chemical energy of the raw coal, calculated according to Eq. (7):

$$\eta = \frac{V_{gas} \cdot LHV_{gas}}{V_{coal} \cdot LHV_{coal}} \cdot 100\% \tag{7}$$

where η (%) represents the gasification efficiency; LHV_{coal} (MJ/kg) represents the lower heating value of the raw coal.

Table 3
The lower heating value of commonly used combustible gases.

Gas	H_2	CO	CH_4	C_2H_4	C_2H_6	C_3H_6	C_3H_8
LHV (MJ/Nm^3)	10.79	12.64	35.88	59.44	64.35	87.61	93.18

2.3.4. Syngas flow rate and syngas conversion rate

The flow rate of the syngas obtained by partial gasification is determined according to the nitrogen balance method [27]. The flow rate of syngas can be calculated based on the volume content of nitrogen in the syngas, as shown in Eq. (8):

$$V_{gas} = \frac{100 \cdot V_{N2}}{X_{N2}} \tag{8}$$

where V_{gas} (L/min) represents the flow rate of the syngas; V_{N2} (L/min) represents the flow rate of nitrogen in the input gas; X_{N2} (%) represents the volume fraction of nitrogen in the syngas.

The reaction time for the partial gasification experiment is 2 min. The syngas conversion rate during the partial gasification process is defined as the ratio of the carbon content in the syngas to the carbon content in the coal, as shown in Eq. (9):

$$\alpha_C = \frac{V_{gas} \cdot C_{gas}}{V_{coal} \cdot C_{ad}} \cdot 100 = \frac{V_{gas} \sum \frac{X_n}{22.4} \cdot 12}{V_{coal} \cdot C_{ad}} \cdot 100\% \tag{9}$$

where α_C (%) represents the syngas conversion rate; V_{gas} (L/min) represents the flow rate of gasified syngas; X_n (%) represents the volume fraction of 1 times CO, CO_2, CH_4, 2 times C_2H_4 and C_2H_6, and 3 times C_3H_6 and C_3H_8 in the syngas; V_{coal} (g/min) represents the coal feeding rate; C_{ad} (%) represents the carbon content of the coal; C_{gas} (%) represents to the carbon content of the syngas.

2.4. Char characterization and data processing method

2.4.1. Combustion characteristics char

To investigate the effect of ER on the combustion characteristics and reactivity of char, this study utilized an automatic sampling synchronous thermal analysis system (Mettler TGA/DSC 3+, Switzerland) to determine the combustion reactivity and characteristics of char[28–30]. Each measurement used a 6 mg char sample. The reactor was initially heated from room temperature to 105 °C at 10 °C/min under an N_2 atmosphere, holding for 15 min to remove residual moisture. The sample was then

heated to 950 °C at 10 °C/min in an air atmosphere with a flow rate of 60 mL/min. The temperature at which the carbon conversion rate of char reached 50 % (dry ash-free basis) was recorded as $T_{0.5}$ to characterize the reactivity of the char. A higher $T_{0.5}$ indicates lower combustion reactivity of the char. The combustion characteristic indicators of char were assessed by the standard GB/T 33,304-2016, including ignition temperature T_i (°C), burnout temperature T_f (°C), maximum burning rate temperature T_p (°C), maximum burning rate $(dw/dt)_{max}$ (%/min) and average burning rate $(dw/dt)_{average}$ (%/min).

2.4.2. Chemical structure of char

To investigate the effect of ER on the chemical structure of char, a Raman spectrometer (Horiba LabRAM HR Evolution, Japan) was used to analyze the crystallinity and ordering of the internal structure of char [31]. The spectrometer employs an argon ion excitation light source (512 nm) to obtain spectra in the range of 4000–100 cm^{-1} [32]. The first-order Raman spectrum (1800–800 cm^{-1}) was fitted with ten Gaussian peaks using *Peak Fit V4.12* software [33,34]. The properties of char samples can be evaluated based on the intensity or ratio of different characteristic peaks. According to a summary of Raman peak/band assignments (Table S1), the G band represents aromatic ring vibration, while the D band corresponds to larger aromatic ring groups (ring number >6) in the char. The three bands between the G and D bands, including G (1540 cm^{-1}), V_L (1465 cm^{-1}), and V_r (1380 cm^{-1}), mainly represented typical structures in amorphous carbon, especially small aromatic ring groups (ring number 3–5). Therefore, the area ratios, I_{total}, $I_{(Gr + VL + Vr)}/I_D$ and I_G/I_D, can be used to characterize the degree of disorder of char, the ratio of small aromatic ring groups to large aromatic ring groups in char and the graphitization of char.

To further investigate surface functional groups and validate the Raman results, Fourier transform infrared spectroscopy (FTIR) was conducted using a Thermo Scientific Nicolet iS20 spectrometer (USA) with a 4000–400 cm^{-1} wavelength range. The potassium bromide (KBr) tablet method was applied, with a mixing ratio of 1:200 between the experimental sample and KBr powder and a total sample mass of 160 mg [35]. According to the band assignments of the FTIR spectra (Table S2), the characteristic peaks can be categorized into hydroxyl groups (3600-3000 cm^{-1}), aliphatic hydrocarbons (3000-2700 cm^{-1}), oxygen functional groups (1800-1000 cm^{-1}) and aromatic hydrocarbons (900-700 cm^{-1}) [36,37]. These bands were fitted to the peaks by the *Peak fit V4.12* software. The integrated area of the fitted peaks was employed for semi-quantitative calculations of the content of each functional group, as outlined in Eq. (10)-Eq. (12) [36,38].

$$\frac{A_{-OH}}{A_{-O-}} = \frac{I_{3550-3250cm^{-1}}}{I_{1300-1000cm^{-1}}} \tag{10}$$

where $I_{x-ycm^{-1}}$ represents the integral areas of the individual characteristic peaks obtained by peak fitting from x cm^{-1} to y cm^{-1}; A_{-OH}/A_{-O-} represents the relative contribution of the hydroxyl stretching band to the ether group, i.e., the conversion of the unstable reactive oxygen-containing functional group to the stabilizing group during pyrolysis. A larger ratio implies a decrease in ether groups and an increase in hydroxyl groups.

$$\frac{A_{C=O}}{A_{-ar}} = \frac{I_{1770-1660cm^{-1}}}{I_{1660-1580cm^{-1}}} \tag{11}$$

$A_{C=O}/A_{-ar}$ represents the relative contribution of carbonyl or carboxyl groups to the aromatic groups, i.e., dissociation and loss of reactive oxygen-containing groups. A larger ratio implies a larger amount of reactive oxygenated groups in the char.

$$\frac{A_{-CH_2}}{A_{-CH_3}} = \frac{I_{2935-2910cm^{-1}}}{I_{2975-2950cm^{-1}}} \tag{12}$$

A_{-CH_2}/A_{-CH_3} represents to the aliphatic chain length and the degree of branching of aliphatic side groups in the char. A larger ratio implies the presence of long-chain carbon structures in the char.

$$\frac{A_{-al}}{A_{-ar}} = \frac{I_{3000-2785cm^{-1}}}{I_{1605-1570cm^{-1}}} \tag{13}$$

A_{-al}/A_{-ar} represents the relative contribution of the aliphatic stretching bands to the aromatic out-of-plane bending mode, i.e., the aromaticity of the char. A larger ratio implies lower aromaticity.

2.4.3. Physical characteristics of char

To investigate the pore characteristics of char, a fully automatic specific surface and porosity analyzer (Micromeritics ASAP 2460, USA) was used to measure char. The pore structure characteristics of char were measured using the N2 adsorption method. The degassing temperature for the test was 300 °C and the degassing time was 7 h.

2.5. Major gasification reaction equations

In the process of coal partial gasification, two distinct types of reactions occur: gas-solid reactions and gas-gas reactions. The specific reaction equations are shown in Eqs. R1-R12 [39,40]:

Gas-solid reactions:

$$C + 0.5O_2 = CO, \Delta H = -110.6\ kJ/mol \quad R1$$

$$C + O_2 = CO_2, \Delta H = -393.6\ kJ/mol \quad R2$$

$$C + H_2O = H_2 + CO, \Delta H = 131.3\ kJ/mol \quad R3$$

$$C + CO_2 = 2CO, \Delta H = 172.5\ kJ/mol \quad R4$$

$$C + 2H_2 = CH_4, \Delta H = -74.9\ kJ/mol \quad R5$$

gas-gas reactions:

$$H_2 + 0.5O_2 = H_2O, \Delta H = -241.9\ kJ/mol \quad R6$$

$$CO + 0.5O_2 = CO_2, \Delta H = -283\ kJ/mol \quad R7$$

$$CO + H_2O = H_2 + CO_2, \Delta H = -41.2\ kJ/mol \quad R8$$

$$CO + 3H_2 = CH_4 + H_2O, \Delta H = -206.2\ kJ/mol \quad R9$$

$$2CO + 2H_2 = CH_4 + CO_2, \Delta H = -203.3\ kJ/mol \quad R10$$

$$CO_2 + 4H_2 = CH_4 + 2H_2O, \Delta H = -208.9\ kJ/mol \quad R11$$

$$CH_4 + 2O_2 = CO_2 + 2H_2O, \Delta H = -866.9\ kJ/mol \quad R12$$

$$2C_nH_m + (2n + m/2)O_2 = 2nCO_2 + mH_2O, \text{exothermic} \quad R13$$

$$C_nH_m + nH_2O = nCO + (n + m/2)H_2, \text{endothermic} \quad R14$$

3. Results and discussions

3.1. Effect of air equivalence ratio on gasification performance

3.1.1. Effect of air equivalence ratio on partial gasification product yield and gas composition

To investigate the effect of ER on the syngas composition obtained after SC partial gasification, a gas chromatograph (GC, Agilent 7890B, USA) was utilized for quantitative analysis of the main components in the syngas. The gas chromatograph is equipped with two thermal conductivity detectors (TCDs) and a hydrogen flame ionization detector (FID). The TCDs can be used to detect CO, CO_2, CH_4, O_2, N_2 and H_2, while the FID can be used to detect CH_4, C_2H_4, C_2H_6, C_3H_6, and C_3H_8.

The composition and yields of the syngas obtained from SC partial gasification at different ER are depicted in Fig. 2. As shown in the figure, the yields (ml/g) of almost all different gas components in syngas

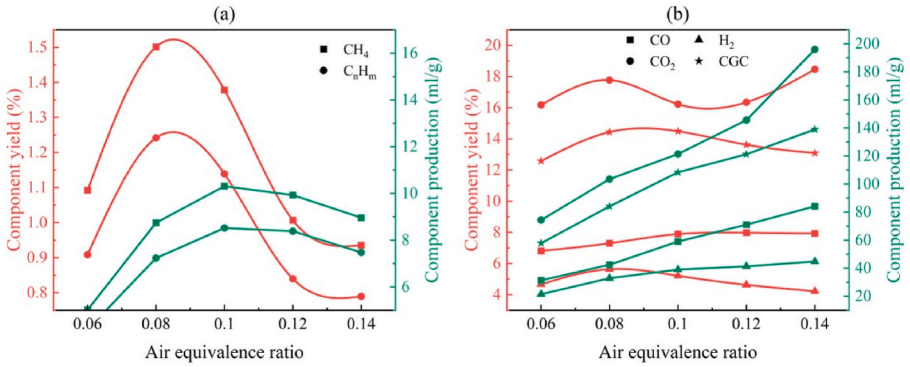

Fig. 2. Gas composition and yield of syngas from coal partial gasification under different ER.

increased with the rising air equivalence ratio (ER). This can be attributed to the increased oxygen availability for the partial gasification reaction, which leads to greater consumption of fixed carbon in the SC and the increasing gas yield. Notably, the yields of CH_4 and C_1-C_3 alkanes initially decreased and then increased as ER increased. This indicates that when the ER exceeds 0.1, the formation rate of CH_4 is lower than its consumption rate. C_1-C_3 alkanes primarily originate from the cleavage and hydrogenation of macromolecular aliphatic side chains with high activity in the coal [41], a process that predominantly occurs during pyrolysis. As ER increases, the percentage content (%) of CH_4 initially rises and then decreases. This is similar to the changing trend of the yields of C_1-C_3 alkanes. When ER exceeds 0.08, gasification takes a dominant position, leading to a decline in CH_4 content in the syngas which indicates that CH_4 is sensitive to the presence of O_2. Simultaneously, the reaction rate of R10 increases with temperature. When ER is too high, the reaction equilibrium of R12 shifts positively, resulting in the consumption of CH_4. Due to changes in the synthesis and combustion rates of CH_4, its content first increases and then decreases. The content of hydrocarbon C_nH_m also shows a trend of initial increase followed by a decrease as ER increases. C_nH_m primarily originates from coal pyrolysis. With an increase in ER, the gasification reaction intensifies, raising the temperature and increasing C_nH_m content. However, when ER exceeds 0.08, excessive oxygen involvement shifts the reaction equilibrium of the combustion reaction R13 and the steam reforming reaction R14 to the positive direction. This increases the decomposition rate of C_nH_m, leading to a decrease in its content. When ER continues to increase, the tar and straight-chain hydrocarbons produced by gasification undergo secondary cracking so that more hydrocarbon C2 is generated [42]. This causes the rate of decrease in C_nH_m to slow after ER exceeds 0.1.

Meanwhile, the content of combustible gas components (CGC) such as H_2, CO and C_1-C_3 alkanes in the syngas ranges between 12.6 % and 14.5 %. With an increase in ER, it first rises and then falls. The high percentage content of CGC, 14.4 % and 14.5 %, occurs at ER of 0.08 and 0.1, respectively. This is due to the transition of the reaction from being dominated by pyrolysis to being dominated by gasification as ER increases which leads to CGC in the syngas increases. However, further increases in ER lead CGC to combust with oxygen, resulting in a decrease in the percentage content of CGC. In the early stages of ER increase, the percentage content of CO rises. However, when ER reaches 0.1, the increase in CO content becomes less pronounced. CO primarily results from reaction R1 [39]. As ER increases, the involvement of O2 rises which elevates the temperature and accelerates the rate of R1. Overall, the CO content increases initially before stabilizing. This slightly deviates from the conclusion of Chen et al. [43] who reported that the CO yield decreases with an increase in the oxygen-coal ratio. This discrepancy is likely since O_2 not only reacts with carbon in coal to form CO but also facilitates the conversion of CO to CO_2 via reaction R7 as the reaction rate of R1 reaches a certain threshold at ER 0.1. As ER increases further, CO_2 content first increases, then decreases and finally rises again. The downward trend in CO_2 content occurs because pyrolysis dominates this stage [39] and the heat provided by partial gasification also accelerates the pyrolysis reaction.

As ER increases, the content of H_2 initially rises and then decreases. On the one hand, because of the increased ER, the temperature continues to rise while accelerating the gasification. This enhances the reaction rate of R14 and shifts the reaction equilibrium in the positive direction, thereby promoting the increase in the content of H_2. On the other hand, the involvement of O_2 in the reaction combusts with the H_2 produced during the process, reducing the content of H_2 and generating more water. Consequently, the content of H_2 exhibits an initial increase followed by a decrease.

Fig. 3 illustrates the trend of syngas, char and tar yields with increasing ER in the partial gasification experiment. It can be seen that both char and tar yields decrease as ER increases. This decrease can be attributed to the acceleration of the coal gasification reaction, leading to the rapid release of volatile matter from the coal and enhancing the reaction rates of R1, R2, and R4. Moreover, higher ER can promote secondary reactions. As ER increases, it facilitates the secondary cracking and oxidation of tar, reducing the tar yield from 9.41 % to 6.87 %. Due to the intensification of coal gasification and the secondary cracking of tar, the syngas yield increases with ER increase. This is consistent with the observed trend of increasing yields of different gas components in the syngas, as analyzed earlier.

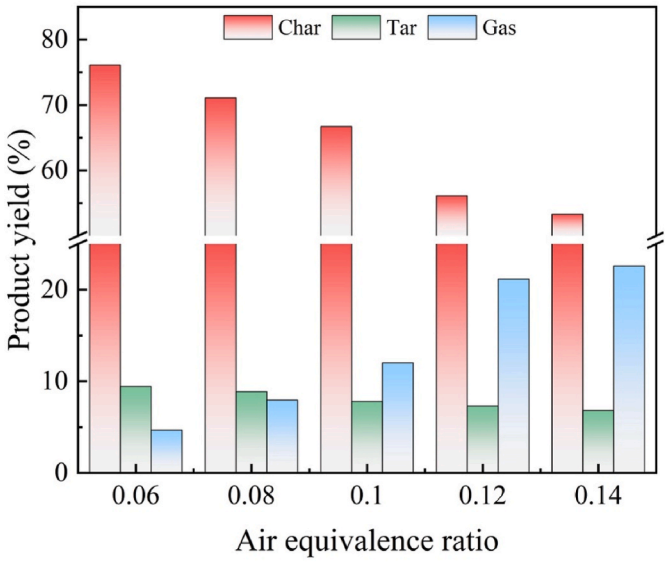

Fig. 3. Partial gasification product yield from coal partial gasification under different ER.

3.1.2. *Effect of air equivalence ratio on* LHV_{gas}, η, V_{gas} *and* α_C

Fig. 4 shows partial gasification indexes of coal partial gasification under different ER. The results indicate that the syngas conversion rate is highly sensitive to ER. As ER increases, the syngas conversion rate rises from an initial 9.22 % to a maximum of 24.09 %. This increase is attributed to the shift in the gasification process of SC from being dominated by pyrolysis at the beginning to being dominated by gasification at higher ER. This shift leads to a more complete volatile analysis and secondary cracking of the tar produced by the reaction, thereby enhancing the syngas yield and syngas conversion rate α_C. As shown in Fig. 4(a), the LHV_{gas} initially increases and then decreases with rising ER. This trend is consistent with the percentage content of CGC in syngas discussed in Section 3.1.1. The CGC in the syngas initially increases and then decreases with ER, leading to changes in LHV_{gas}. At an ER of 0.08, the LHV_{gas} reaches its peak at 2.15 MJ/Nm^3.

As shown in Fig. 4(b), with increasing ER, both gasification efficiency η and syngas flow rate V_{gas} exhibit a continuous upward trend. At an equivalence ratio of 0.14, these two gasification parameters peak at 50.77 % and 5.11 L/min, respectively. This increase is primarily due to the elevated ER promoting higher reaction temperatures and the combustion of fixed carbon, facilitating the complete release of volatiles from SC and the conversion of fixed carbon into syngas. As ER rises, more oxygen participates in the oxidation reactions of coal, tar, and syngas. Although this results in a decrease in syngas calorific value, the yield of syngas increases which finally leads to η. The increased participation of O_2 in these reactions also results in an upward trend in the syngas flow rate V_{gas} observed in the partial gasification experiments.

3.2. *Effect of air equivalence ratio on the characteristics of tar*

To investigate the effect of the ER on the characteristics of tar obtained from partial gasification, a GC-MS (Agilent 7890B, USA) was used to analyze tar. The gas chromatographic column used was an HP-5ms capillary column, with high-purity helium flowing at 1.14 mL/min as the carrier gas. The tar detection data were qualitatively analyzed using the NIST-2017 database [44]. The matching factors of all detected components of tar were above 90 %. The relative content of each component was calculated by area normalization.

Fig. 5 shows the GC-MS spectrum of tar from coal partial gasification under different ER. To quantitatively analyze the changes in tar components, the peak areas of different characteristic peaks in the total spectrum are typically used to represent the relative contents of various major components in tar [45]. Using the NIST database system, compounds with the highest probability of matching characteristic chromatographic peaks were identified and the main compounds in tar were categorized into five groups: polycyclic aromatic hydrocarbons, monocyclic aromatic hydrocarbons and derivatives, aliphatic hydrocarbons, aliphatic hydrocarbon derivatives and phenols. As shown in Fig. 5, different numbers and colors denote the categories of various major components, with their relative contents quantitatively calculated based on peak areas. The identified main compounds and their contents are listed in Table S3. Additionally, the compounds are classified into four categories based on the number of carbon atoms (C) present in the main compounds in tar: C_1-C_{10}, C_{11}-C_{15}, C_{16}-C_{20} and $>C_{20}$.

Fig. 6 shows the relative content of different organic matter in tar. As shown in Fig. 6(a), the phenols and monocyclic aromatic hydrocarbons and their derivatives dominate the main components of the tar obtained after partial gasification, accounting for 38.23%–45.52 % and 28.37%–32.39 %, respectively. This differs from the dominance of aromatic hydrocarbons and aromatic hydrocarbon derivatives in the pyrolysis process. This is because the presence of oxygen in the gasification process introduces free hydroxyl and carbonyl groups, promoting reactions with hydroxyl radicals in the coal, which leads to the formation of phenolic compounds. Additionally, the introduction of oxygen accelerates the cracking of large aromatic ring compounds, resulting in an increased generation of phenolic compounds.

The content of phenolic compounds in the tar decreases and then increases with increasing ER. At lower ER, phenolic compounds are generated in larger quantities during pyrolysis. However, as the oxygen content increases, oxidation reactions occur, forming phenolic aldehydes, phenolic ketones, and other products, leading to a decrease in phenolic content. As ER increases further, the decomposition of SC and its tar generates volatile compounds containing active oxygen groups, which react with aromatic ring side chains and bridges to form more phenolic compounds [46]. Additionally, aromatic compounds undergo rearrangement or cracking at higher ER, resulting in increased phenolic concentrations, such as phenol. At this stage, the formation of phenolic compounds exceeds their oxidation rate, causing an increase in the subsequent phenolic compound content.

As shown in Fig. 6(a), the overall content of aliphatic hydrocarbons and their derivatives decreases as the decomposition of heavier products with higher reactivity, such as long-chain aliphatic hydrocarbons, accelerates with increased oxygen content. This breakdown promotes the formation of smaller molecular gases and other compounds. During the transformation of aliphatic hydrocarbons and their derivatives, the decrease in the content of aliphatic hydrocarbon derivatives is more pronounced, with a maximum reduction of 2.79 %. This can be attributed to the poor structural stability of hydrocarbon derivatives containing heteroatom structures [47] which decompose more readily at high temperatures. The content of polycyclic aromatic hydrocarbons and monocyclic aromatic hydrocarbons and derivatives follows a trend of first increasing and then decreasing, reaching maximum levels at ER values of 0.08 and 0.1, respectively. Initially, at low ER, the concentration of polycyclic aromatic hydrocarbons increases. This may be partly due to the polymerization of highly reactive monocyclic aromatic hydrocarbons and their derivatives, which form polycyclic aromatic hydrocarbons. Additionally, some free radical fragments from the oxidation of aliphatic hydrocarbons and their derivatives may promote the polymerization reaction, forming polycyclic aromatic hydrocarbons. At higher ER, polycyclic aromatic hydrocarbons undergo oxidation and

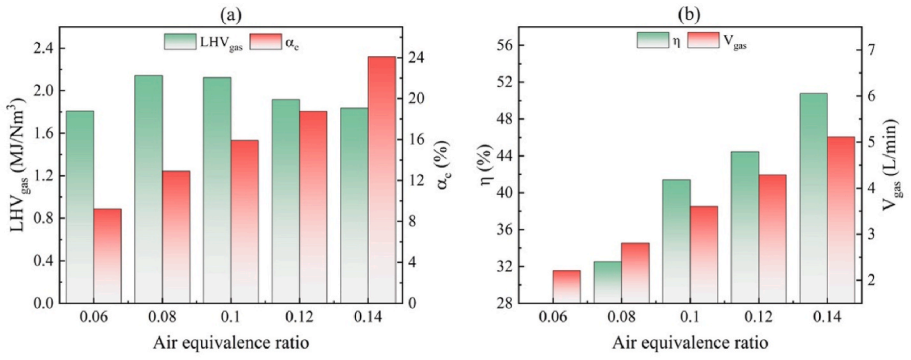

Fig. 4. Partial gasification indexes of coal partial gasification under different ER.

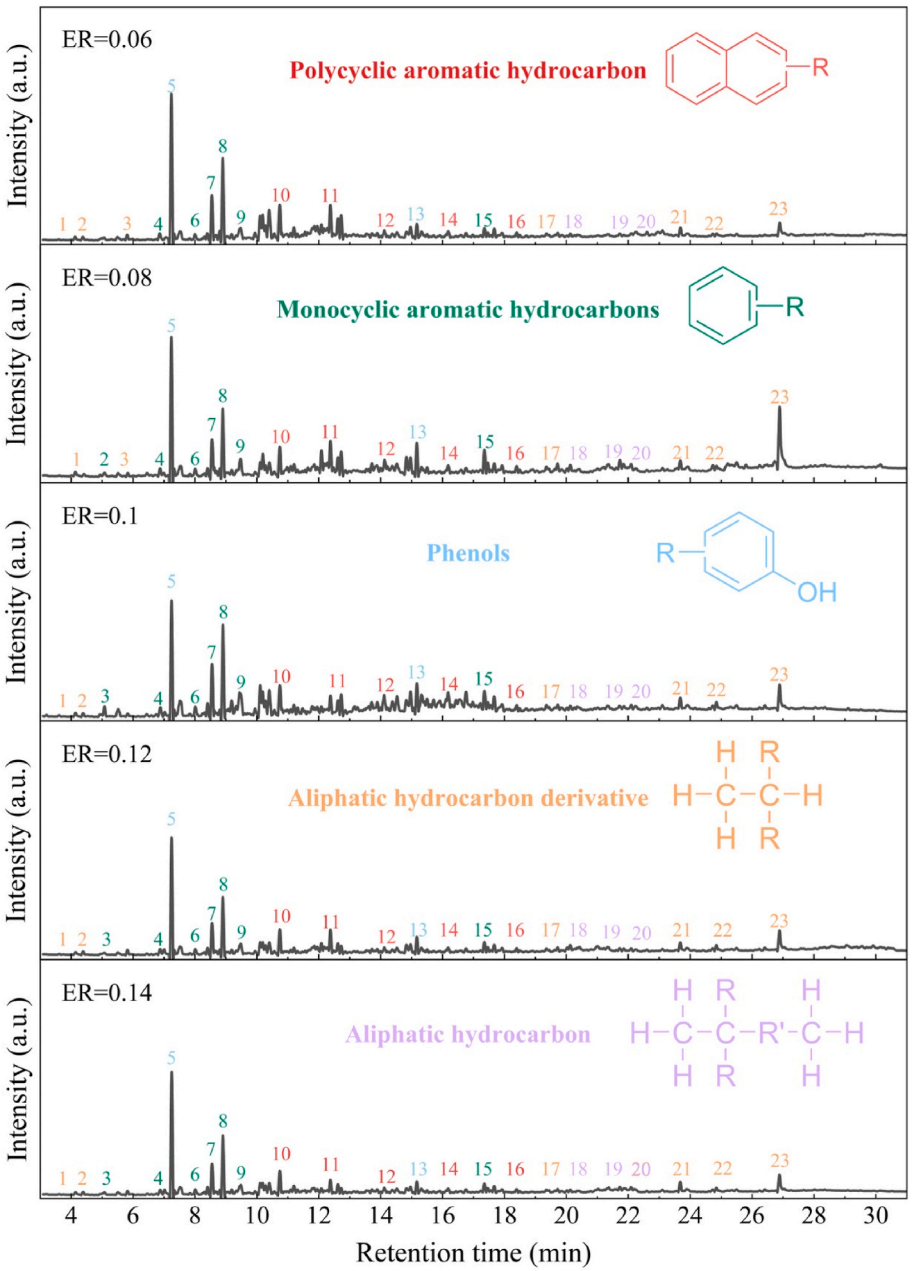

Fig. 5. GC-MS spectrum of tar from coal partial gasification under different ER.

cracking, resulting in the formation of monocyclic aromatic hydrocarbons and a decrease in the content of polycyclic aromatic hydrocarbons. At this stage, the content of phenolic compounds decreases, with phenol and similar substances likely undergoing oxidation to form monocyclic aromatic compounds. Consequently, the concentration of monocyclic aromatic hydrocarbons increases initially as the ER rises, peaking at an ER of 0.1. Notably, at an ER of 0.1, the content of phenolic compounds reaches its lowest point, indicating that a portion of these compounds has been converted into monocyclic aromatic compounds. With a further increase in ER, the concentration of monocyclic aromatic hydrocarbons and their derivatives decreases and stabilizes but remains higher than at an ER of 0.06. This phenomenon can be explained by the continued decomposition of polycyclic aromatic hydrocarbons into monocyclic aromatic hydrocarbons and derivatives which then undergo rearrangement to phenolic compounds and other compounds. These two reasons ultimately lead to a decrease in the content of monocyclic aromatic hydrocarbons and derivatives, which then stabilizes.

As shown in Fig. 6(b), the main compounds below C10 in the tar obtained from the partial gasification occupy a dominant position, accounting for 72.13 %–79.92 %. This proves that the introduction of oxygen can cause the decomposition of long-chain structures and polycyclic aromatic hydrocarbon structures into short-chain structures and monocyclic aromatic hydrocarbon compounds during the gasification process. There is a rising trend in the major compound content below C_{10} and in the C_{16}–C_{20} range as ER increases. Concurrently, the content of main compounds above C_{20} in the tar shows a significant downward trend, with the largest decrease being 3.95 %. In contrast, the content of main compounds in the C_{11}-C_{15} range initially increases and then decreases. It primarily consists of polycyclic aromatic hydrocarbons (such as $C_{11}H_{10}$, $C_{12}H_{12}$, $C_{13}H_{14}$) and a phenolic compound ($C_{14}H_{22}O$). As previously mentioned, polycyclic aromatic hydrocarbons decrease with increasing ER, while phenolic compounds first decrease and then increase. Therefore, the content of C_{11}-C_{15} compounds in the tar shows a decreasing trend.

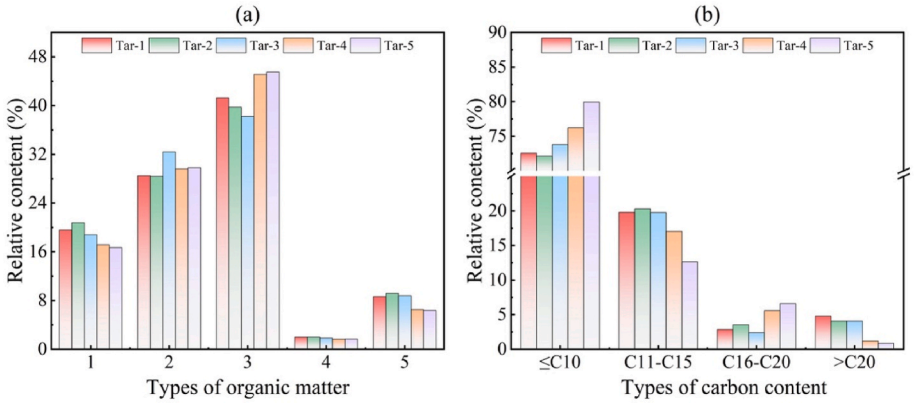

Fig. 6. Relative content of different organic matter in tar
Note: Tar-1 to Tar-5 represent the tar prepared at air equivalent ratios of 0.06–0.14, respectively; The horizontal axes 1, 2, 3, 4, and 5 in Figure (a) represent polycyclic aromatic hydrocarbons, monocyclic aromatic hydrocarbons and their derivatives, phenols, aliphatic hydrocarbons, and aliphatic hydrocarbon derivatives, respectively.

3.3. Effect of air equivalence ratio on the characteristics of char

3.3.1. Combustion characteristic

Fig. 7 shows the TG curves of char from coal partial gasification under different ER, along with the values of $T_{0.5}$. The results indicate that with an increase in ER, the $T_{0.5}$ of the char increases, suggesting a decline in the combustion reactivity of the char. $T_{0.5}$ rose from 424.5 °C at an ER of 0.06–439.9 °C at an ER of 0.14. This trend can be attributed to the gasification process during which the volatiles remaining in the char are burned and the combustion of fixed carbon. As shown in Table 4, the results of the proximate, ultimate and calorific value analysis of char samples indicate that with the increase in ER, the residual volatile matter and fixed carbon content in the char samples decrease, leading to worsened combustion performance. However, the extent of the change in $T_{0.5}$ is not significant, possibly because the gasification reaction increases the pore volume of the char which enhances its specific surface area and creates more active sites on the coal surface. Elemental analysis reveals that the proportions of C, H, and O in the char decrease with increasing ER, suggesting that the partial gasification of SC is a process of dehydrogenation, deoxygenation, and carbon enrichment. The reduction in these three elements and the volatile matter content of the char leads to a decrease in the lower heating value as ER increases with the highest heating value of 27.34 MJ/kg when ER is 0.06.

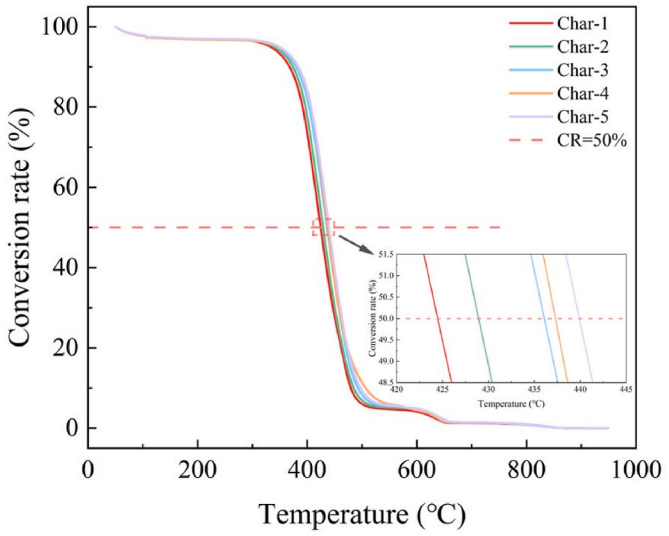

Fig. 7. TG curves and combustion reactivity of char from coal partial gasification under different ER
Note: Char-1 to Char-5 represent the char prepared at air equivalent ratios of 0.06–0.14, respectively.

Fig. 8 shows the TG and DTG curves of char under different ER and combustion indicators. The DTG graph reveals two main weight loss peaks within the temperature range of 50–950 °C. The first peak occurs at 420.9–439.2 °C, which corresponds to the maximum combustion rate temperature (T_p). This peak can be attributed to the

Gasification reaction of char, complete volatilization of gases and the oxidation of fixed carbon. The second peak appears at 640–650 °C, attributed to the secondary reaction of char gasification. Some relatively stable macromolecular substances, such as ethers, remain in the char and require higher temperatures and sufficient oxygen to decompose and be consumed. As ER increases, both weight loss peaks of char shift towards higher temperatures. The three combustion characteristic temperatures also show an increasing trend, with the maximum change observed in T_p which rises from 420.9 °C to 439.2 °C. The maximum combustion rate $(dw/dt)_{max}$ remains relatively constant within the range of 10–11.2 %/min. The average combustion rate $(dw/dt)_{average}$ shows a downward trend from 8.1 %/min to 7.2 %/min. This behavior is consistent with the earlier observations, as an increased ER results in more volatile matter and fixed carbon in the partially gasified char being precipitated and oxidized, thereby increasing the ignition temperature and slowing the combustion rate post-ignition.

3.3.2. Chemical structure

As shown in Fig. 9(a), the fitting of the Raman spectrum curve for char prepared at an ER of 0.1 exhibited an excellent result, with the fitting regression coefficient (R^2) exceeding 0.99. The total peak intensity I_{total} of the Raman spectrum from 1800 cm^{-1} to 800 cm^{-1} is calculated by summing the fitting areas of the 10 Raman peaks. This parameter characterizes the degree of disorder in the sample: the larger the I_{total}, the higher the degree of disorder. The specific results of the three characteristic parameters: total Raman peak intensity I_{total}, Raman band area ratio $I_{(Gr + VL + Vr)}/I_D$ and I_G/I_D for each char sample are calculated based on the area parameters of each Gaussian peak obtained by fitting, as shown in Fig. 9(b). The results indicate that with increasing ER and gasification temperature, the total peak intensity I_{total} of char initially rises and then falls, peaking at an ER of 0.1. The value of I_{total} is predominantly influenced by the light absorption capability of the sample, Raman scattering ability and the presence of oxygen-containing components which can induce resonance effects [33,34]. Electron-rich structures, such as oxygen-containing functional groups, generally exhibit higher Raman scattering ability. Therefore, if the reaction

Table 4
Proximate, ultimate and calorific value analysis of char samples.

Sample	Proximate analysis (ad, wt%)				Ultimate analysis (ad, wt%)					LHV (MJ/kg)
	M	A	V	FC	C	H	N	S_t	O_{diff}	
Char-1	3.19	13.09	11.69	72.03	70.12	2.00	0.85	0.25	10.50	27.34
Char-2	3.11	14.31	11.40	71.18	68.60	1.97	0.81	0.21	10.99	26.27
Char-3	3.06	16.41	10.93	69.60	68.93	1.96	0.96	0.17	8.52	25.51
Char-4	2.72	18.62	9.23	69.43	67.84	1.75	0.81	0.16	8.11	25.48
Char-5	2.52	20.98	9.17	67.33	65.86	1.62	0.82	0.19	8.01	24.49

Note: (1) M: Moisture, A: Ash, V: Volatile, FC: Fixed carbon; (2) ad: Air dry basis, t: Total, diff: By difference.

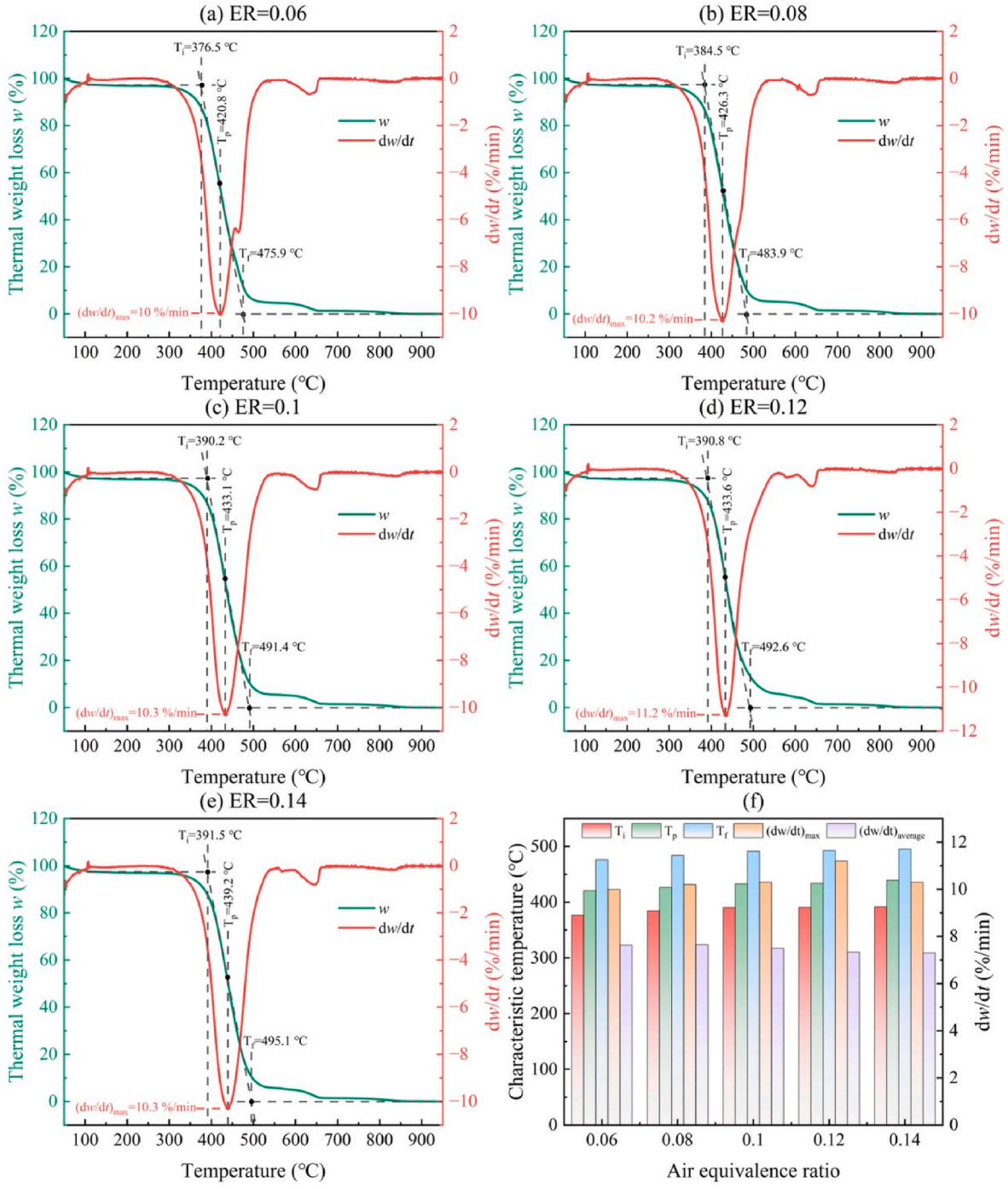

Fig. 8. TG, DTG curves and combustion characteristic indicators of char from coal partial gasification under different ER.

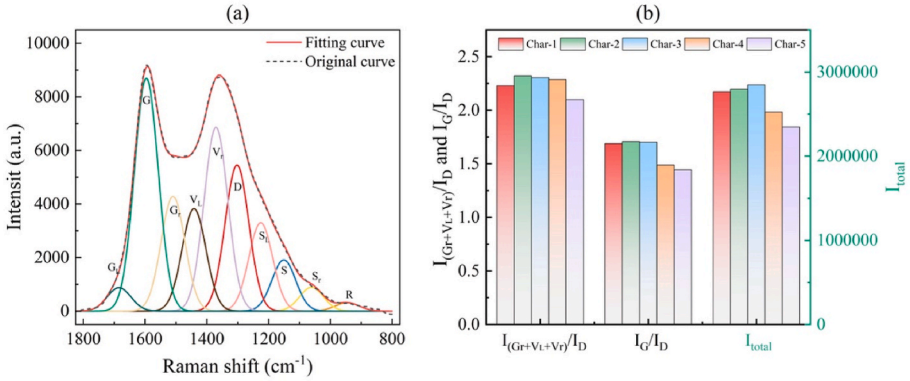

Fig. 9. (a) Peak fitting examples of Raman spectra; (b) Raman characteristic parameters of char.

consumes more oxygen-containing functional groups, the I_{total} value decreases. This indicates that in the ER range of 0.06–0.1, increasing the ER enhances the oxygen-containing functional groups in the char, thereby increasing the degree of disorder and the I_{total} value. If the ER increases further, some of the more active oxygen-containing functional groups in the char, such as hydroxyl and carbonyl, will be further consumed, leading to increased order and a reduction in the I_{total} value.

The ratio of the Raman band areas of the ($G_r + V_L + V_r$) band to the D band, $I_{(Gr + VL + Vr)}/I_D$, can reflect the ratio of small aromatic ring groups (ring number 3–5) to large aromatic ring groups (ring number >6) in char [29]. As shown in Fig. 9 (b), $I_{(Gr + VL + Vr)}/I_D$ exhibits a trend of first increasing and then decreasing. At low ER, the pyrolysis reaction predominates, causing the large aromatic ring structure to decompose and generate more small aromatic ring structures, leading to a slight increase in the $I_{(Gr + VL + Vr)}/I_D$ value. As ER continues to increase, the char selectively consumes smaller aromatic ring structures, decomposing them into products such as oxygen-containing functional groups or condensing them into large aromatic ring structures which make the residual char more condensed [30]. As the gasification reaction becomes more complete and the number of small aromatic ring groups decreases, resulting in a decrease in the $I_{(Gr + VL + Vr)}/I_D$ value. Additionally, with an increase in ER, the amount of CO_2 generated by partial gasification also increases. On the one hand, CO_2 participates in cross-linking reactions on the surface of char, attaches to coal and expands the pore size of the micropores and mesopores of char [48]. This increases the active sites on the surface of coal and leads to the formation of more oxygen-containing functional groups. These functional groups are more likely to desorb through the breaking of C-C bonds, thereby generating smaller aromatic ring structures and long-chain aliphatic structures. On the other hand, long-chain aliphatic structures produce steric groups that inhibit the condensation of small aromatic ring structures [49], resulting in an increase in small aromatic ring structures and an indirect decrease in large aromatic ring structures. Hence, the $I_{(Gr + VL + Vr)}/I_D$ value decreases slowly at first.

The ratio of the Raman band areas of the G band to the D band, I_G/I_D, can reflect the degree of graphitization of the carbon structure in char [32]. A higher value of I_G/I_D indicates a lower degree of graphitization in the char. The trend of the I_G/I_D value with changing ER is similar to that of $I_{(Gr + VL + Vr)}/I_D$, both showing an initial increase followed by a decrease. This indicates that with increasing ER, the graphitization degree of the char first decreases and then increases. In the beginning, the increase in the I_G/I_D value is small. As described above, although more oxygen-containing functional groups and large aromatic ring structures are generated during the initial increase in ER, many new small aromatic ring structures are decomposed which increases the disorder of the char and reduces its graphitization degree. In this process, due to the introduction of oxygen, more active structures also undergo oxidation reactions, producing gases such as CH_4 and CO which corresponds to the conclusion in Section 3.1.1. When the ER continues to increase, the I_G/I_D value decreases, but the downward trend slows. This is because most of the oxygen-containing functional groups have been consumed during the reaction and the small aromatic ring structures have begun to condense to form larger aromatic ring structures. The width of the D band in the char is very broad, indicating that while there are many sizes of aromatic ring structures, they are insufficient to form graphite crystals [32]. Since these large aromatic ring structures have Raman activity in the D band, the reduction of "defective" structures leads to a relatively low Raman intensity of the D band. Therefore, the subsequent decrease in the I_G/I_D value is relatively small.

Fig. 10 (a) shows the FTIR spectra of different char samples. As shown in the figure, in the wavenumber range of 3600–3000 cm^{-1}, each char sample exhibits a broad and strong characteristic peak around 3430 cm^{-1}, indicating relatively strong hydroxyl vibrations in all samples. This indicates that the presence of phenol, alcohol or water was generated during the reaction process [50]. Notably, all samples exhibit two characteristic peaks with low intensity at 2923 cm^{-1} and 2870 cm^{-1} in the 3000-2700 cm^{-1} range, attributed to the stretching vibrations of methyl groups. These peaks indicate a low content of long-chain aliphatic hydrocarbons in the samples [38]. In the 1800-1000 cm^{-1} region, all samples display several strong and prominent peaks, suggesting the presence of abundant oxygen-containing functional groups in the char. However, variations in peak intensity and number among the samples imply different degrees of decomposition of these groups during the reaction. Additionally, two characteristic peaks at 880 cm^{-1} and 770 cm^{-1} are observed in all samples, assigned to the aromatic ring structures in the char.

Since the characteristic peaks appearing in each spectrum are composed of different functional groups, the information obtained from the total FTIR spectra is only for approximate variations and is not accurate. As shown in Fig. 10(c)–(f), the FTIR curves across different wavenumber ranges are performed through peak fitting and semi-quantitative analysis in this study. The semi-quantitative FTIR ratios are shown in Fig. 10(b). Both A_{-OH}/A_{-O-} and $A_{C=O}/A_{-ar}$ increase and then decrease with increasing ER, reaching their maximum values at an ER of 0.1. This indicates that at low ER, pyrolysis dominates the process. The involvement of oxygen leads to an increase in hydroxyl and other oxygen-containing functional groups in the char which enhances the disorder in its internal structure. This result is consistent with the Raman analysis. As ER increases, O_2 selectively consumes high-reactivity oxygen-containing functional groups through the following mechanisms [51,52]: (1) gasification of small molecules connected by carbonyl groups; (2) decomposition of ether groups producing CO; (3) oxidation of carbonyl, aldehyde, and carboxyl groups producing CO_2; (4) cracking of aliphatic groups. These processes ultimately result in a decrease in the content of these functional groups and the generation of small molecular gases. However, it is observed that at ER of 0.12 and 0.14, the A_{-OH}/A_{-O-} values are nearly identical. This is because A_{-OH}/A_{-O-} is influenced not only by the content of hydroxyl but also by the content of

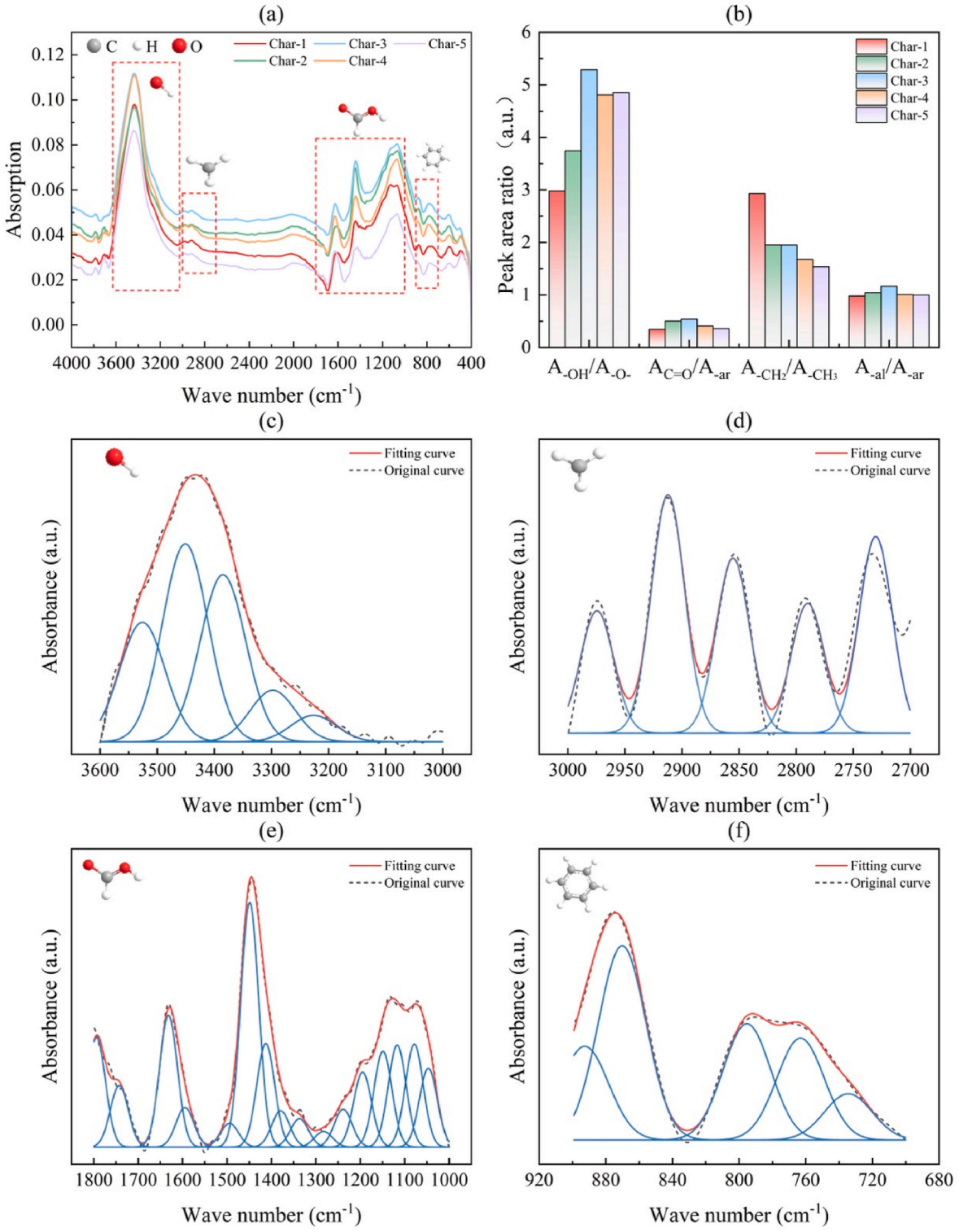

Fig. 10. FTIR analysis of char samples: (a) FTIR curve of char samples; (b) FTIR characteristic parameters of char samples; (c)–(f): Peak fitting examples of FTIR spectra in different wavenumber ranges.

ether which is thermally stable. Moreover, high-reactivity groups like alcohols, phenols and carboxylic acids can convert to ether groups [36] which decompose at a much slower rate than hydroxyl groups. Thus, the consumption rate of ether groups is lower than that of hydroxyl groups, resulting in similar A_{-OH}/A_{-O-} values at ERs of 0.12 and 0.14.

As ER increases, the value of A_{-CH_2}/A_{-CH_3} continuously decreases. The increase in ER leads to a higher concentration of O_2 participating in the reaction and an elevated reaction temperature. And the concentration of free radicals in the reaction process also increases [53]. Therefore, long-chain aliphatic hydrocarbons with poor thermal stability are consumed at a higher rate, generating small molecules such as H_2, C_nH_m, and CO_x [54], leading to a decrease in the A_{-CH_2}/A_{-CH_3} value. The value of A_{-al}/A_{-ar} initially increases and then decreases with increasing ER, following a trend similar to that observed in $I_{(Gr + VL + Vr)}/I_D$ and I_G/I_D.

This suggests that the aromaticity of the char first decreases and then increases with increasing ER. This is consistent with the change in graphitization degree reflected by I_G/I_D. The notion that pyrolysis predominates at low ER is further supported by this. At this stage, the decomposition rate of large aromatic ring structures is faster than the consumption rate of small aromatic rings. However, as ER increases further, small aromatic ring structures are preferentially oxidized and consumed or undergo polymerization into large aromatic ring structures, resulting in their consumption rate exceeding the generating rate, which ultimately leads to the aromaticity of the char decreasing again.

3.3.3. Physical structure

Fig. 11 shows the nitrogen adsorption and desorption isotherms of char produced at different ER. The hysteresis phenomenon observed in the low-temperature nitrogen adsorption isotherm is typically related to capillary condensation in the pore structure. Generally, different adsorbent types and adsorption environments (temperature and pressure) cause hysteresis loops of different shapes [55]. As shown in Fig. 11, the isothermal adsorption-desorption curves of char exhibit H4-type hysteresis loops, indicating that the pore structure inside the char comprises blind pores with one end closed, parallel plate slit pores, narrow crack pores or ink-bottle pores [56]. Additionally, the adsorption isotherms of the char belong to type II isotherms [55]. The reversible type II isotherm is typical for non-porous or macroporous adsorbents, consistent with the fact that the char obtained in this experiment is more dominated by macropores in the pore size distribution curve (see Fig. 11).

The changes in the specific surface area, micropore specific surface area, pore volume and micropore specific surface area of char obtained by partial gasification at different ER are shown in Table 5. As shown from the table, with the increase in ER, the specific surface area and micropore specific surface area of char initially increase and then decrease, while the pore volume and micropore volume show an upward trend. This indicates that with the increase in ER, more oxygen can enter the char to participate in the gasification reaction, making the trend of the specific surface area of char similar to the trend of char disorder with ER. The specific surface area of char reaches a maximum value of 249.904 m^2/g at an ER of 0.1. This suggests that the highly active groups in the char facilitate reactions, thereby accelerating the development of char pores. However, when ER increases from 0.12 to 0.14, the specific surface area and micropore specific surface area of char increase slightly. This may be due to the char gradually undergoing combustion reactions during this process, producing more CO_2 which also participates in the cross-linking reaction within the char, expanding the pore size and specific surface area of the char [48].

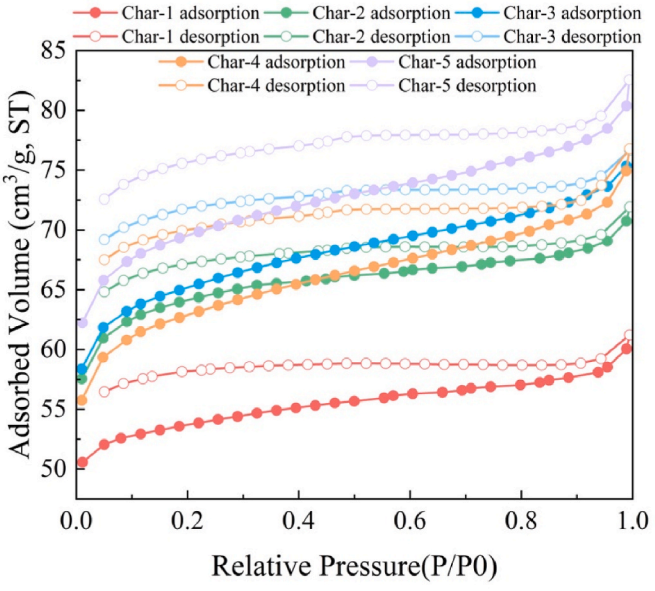

Fig. 11. Adsorption and desorption isothermal hysteresis curves of char.

Table 5
Specific surface area and pore characteristic parameters of coke produced under different ER.

ER	S_{bet} (m^2/g)	S_{mic} (m^2/g)	V_{total} (cm^3/g)	V_{mic} (cm^3/g)
0.06	209.642	188.896	0.0947	0.074
0.08	246.456	212.291	0.111	0.084
0.1	249.904	205.255	0.1186	0.082
0.12	240.638	193.145	0.1188	0.085
0.14	245.205	202.139	0.1277	0.087

Note: S_{bet} is the BET specific surface area; S_{mic} is the micropore specific surface area; V_{total} is the total pore volume; V_{mic} is the micropore volume.

3.4. Effect mechanism of air equivalent ratio on partial gasification products

Experimental results show that changes in ER significantly affect the generation and decomposition of oxygen-containing functional groups in char, thereby altering its internal structure and degree of disorder. Fig. 12 shows a schematic diagram of the mechanism by which ER influences the partial gasification products of SC. The figure illustrates that ER impacts the three primary products of partial gasification: syngas, tar and char. As ER increases, a greater amount of oxygen participates in the partial gasification reaction. The reaction gradually shifts from being dominated by initial pyrolysis to being dominated by gasification. Initially, the content of CGC increases. This is because the increase in oxygen promotes reactions R1, R3, R4 and R14, thereby enhancing coal pyrolysis and leading to a rise in CGC content in the syngas. When the O_2 reaches a certain level, the reaction shifts predominantly towards gasification. This promotes the progress of reactions R2, R6 and R13, resulting in a reduction of CGC content in the syngas and an increase in CO_2.

The macromolecular substances (such as polycyclic aromatic hydrocarbons) and unstable structures (such as aliphatic hydrocarbons and their derivatives) in tar undergo cracking reactions due to the gradual increase in oxygen. These reactions generate short-chain structures, monocyclic aromatic hydrocarbons and derivatives and gases such as CO and CH_4. Simultaneously, the cracking of macromolecular substances produces highly active oxygen-containing functional groups, such as free hydroxyl and carbonyl groups, which elevate the content of phenolic compounds. Phenolic compounds are oxidized to form phenolic aldehydes, phenolic ketones or other oxidation products. When O_2 continues to increase, the oxidation rate of phenolic compounds becomes slower than the cracking rate of macromolecular substances like polycyclic aromatic hydrocarbons, resulting in a trend where phenolic compounds initially decrease and then increase. Tar undergoes secondary cracking reactions at this stage, and the deepening gasification reaction with char increases the yield of syngas to a certain extent. The heavy components (>C20) in tar shift to lighter components (<C10).

As the ER increases, the combustion reactivity of char decreases. The weight loss peak of char shifts toward higher temperatures, the ignition temperature of char increases and the combustion rate decreases after ignition. However, the combustion characteristics of char change slightly. This may be due to the gasification reaction expanding the pore volume of char, increasing the specific surface area of char and creating more vacancy active sites on the coal surface. This causes its combustion reactivity to decrease slowly. Although increasing the ER initially increases the oxygen-containing functional groups and disorder degree inside the char when pyrolysis dominates, during gasification, the more active oxygen-containing functional groups inside the char undergo the following reactions: (1) gasification of small molecules connected by

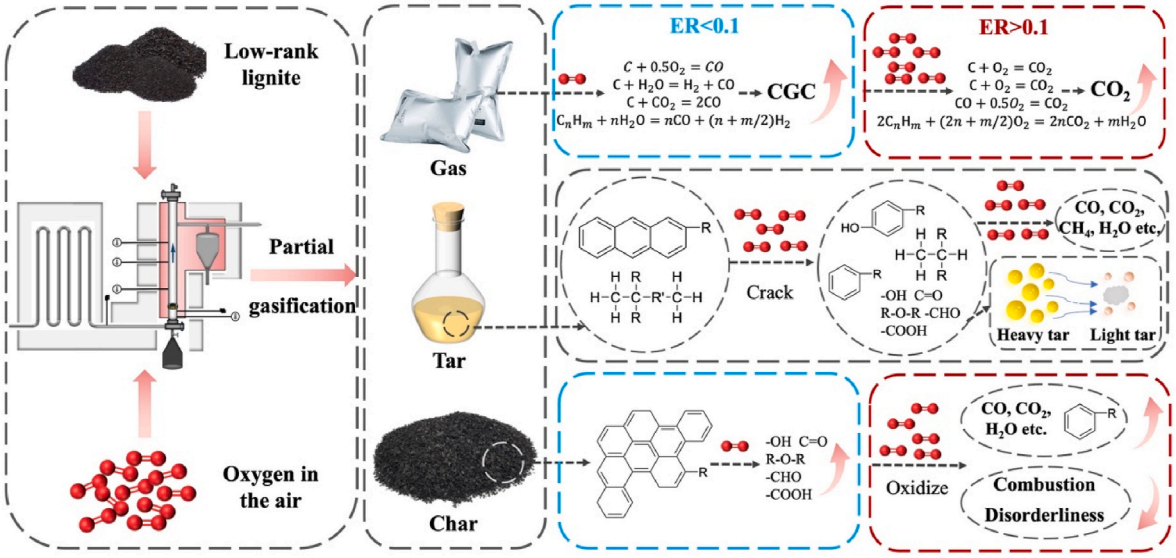

Fig. 12. Schematic diagram of the effect of air equivalence ratio on partial gasification products of SC.

carbonyl groups; (2) decomposition of ether groups to produce CO; (3) decomposition of carbonyl, aldehyde, and carboxyl groups to produce CO_2; (4) decomposition of aliphatic groups. This results in the char becoming more ordered and improves partial gasification efficiency.

4. Conclusion

In this study, a series of partial gasification experiments were conducted using lignite in a self-built fluidized bed, with air serving as the gasifying agent. The effects and mechanisms of the air equivalence ratio (ER) on partial gasification indexes and products were investigated. The main conclusions are as follows.

(1) As the ER increased from 0.06 to 0.14, the dominant reaction of SC shifted from pyrolysis to gasification. The percentage content of CGC such as C_nH_m, H_2 and CO initially increased and then decreased, reaching higher levels at ER of 0.08 and 0.1. Syngas achieved a maximum lower heating value of 2.15 MJ/Nm3 at an ER of 0.08 and a maximum gasification efficiency of 24.09 % at an ER of 0.14.

(2) With increasing ER, tar yield decreased. Higher ER facilitated the cracking of macromolecules like polycyclic aromatic hydrocarbons, leading to the formation of free hydroxyl and carbonyl groups. These reactions promoted the formation of phenolic compounds, causing phenolic compounds and monocyclic aromatic hydrocarbons and derivatives to dominate. The decomposition of long-chain and polycyclic aromatic hydrocarbons into smaller compounds reduced the content of polycyclic aromatic hydrocarbons and aliphatic hydrocarbons, shifting the tar composition from heavier ($>C_{20}$) to lighter ($<C_{10}$) components.

(3) With increasing ER, char yield decreased from 76.1 % to 53.3 %. The higher O_2 concentration intensified oxidation reactions during partial gasification, reducing the combustion reactivity of char. TG analysis showed that the two weight loss peaks of char shifted to higher temperatures with higher ER, though the changes were moderate. This could be attributed to the gasification reaction expanding the pore volume of char which increased its specific surface area and created more vacancy active sites on its surface. This slowed the decrease in combustion reactivity.

(4) ER significantly influenced the formation and decomposition of oxygen-containing functional groups in char, altering its internal structure and degree of disorder. At an ER of 0.1, the content of oxygen-containing functional groups in char was at its highest and the char exhibited the greatest disorder. Beyond an ER of 0.1, additional oxygen participated in combustion reactions. The values of I_{total} and $I_{(Gr + VL + Vr)}/I_D$ first increase and then decrease. Semi-quantitative analysis of FTIR spectra aligned with Raman spectroscopy, showing a consistent trend in oxygen-containing functional groups and char disorder.

CRediT authorship contribution statement

Bin Zhang: Writing – review & editing, Writing – original draft, Visualization, Validation, Methodology, Formal analysis, Data curation, Conceptualization, Guilin Xie, Supervision, Project administration. **Zhihua Tian:** Writing – review & editing, Supervision, Methodology, Conceptualization. **Qinhui Wang:** Supervision, Funding acquisition. **Dong Ma:** Validation, Supervision. **Ruiqing Jia:** Supervision.

Declaration of interest statement

The authors declare that they have no known competing financial interests or personal relationships that could have appeared to influence the work reported in this paper.

Acknowledgement

Thanks for the financial supported by the Fundamental Research Funds for the Central Universities (2022ZFJH004).

Appendix B. Supplementary data

Supplementary data to this article can be found online at https://doi.org/10.1016/j.joei.2025.102008.

References

[1] Statistical Review of World Energy 2024, Energy Institute 3 (2024).
[2] X. Liu, Z. Jin, Y. Jing, P. Fan, Z. Qi, W. Bao, J. Wang, X. Yan, P. Lv, L. Dong, Review of the characteristics and graded utilisation of coal gasification slag, Chin. J. Chem. Eng. 35 (2021) 92–106, https://doi.org/10.1016/j.cjche.2021.05.007.
[3] M. Zhang, Y. Bai, X. Men, X. Song, P. Lv, J. Wang, W. Su, G. Lu, G. Yu, Evolution of oxygen-containing functional groups on coal char surface during gasification in H2O/CO2, J. Energy Inst. 114 (2024) 101622, https://doi.org/10.1016/j.joei.2024.101622.

[4] J. Ma, Characterstics of calcium microstructure evolution during catalytic gasification of shengli lignite. Master, Inner Mongolia University of Technology, 2022, https://doi.org/10.27225/d.cnki.gnmgu.2021.000538.

[5] P. Liu, D. Zhang, L. Wang, Y. Zhou, T. Pan, X. Lu, The structure and pyrolysis product distribution of lignite from different sedimentary environment, Appl. Energy 163 (2016) 254–262, https://doi.org/10.1016/j.apenergy.2015.10.166.

[6] B. Lv, X. Deng, F. Jiao, B. Dong, C. Fang, B. Xing, Enrichment and utilization of residual carbon from coal gasification slag:A review, Process Saf. Environ. Protect. 171 (2023) 859–873, https://doi.org/10.1016/j.psep.2023.01.079.

[7] T. Xu, J. Chen, Y. Wu, X. Gao, S. Bhattacharya, Syngas production from two-step CO2 gasification of low rank coal in an entrained flow reactor, J. Energy Inst. 103 (2022) 169–176, https://doi.org/10.1016/j.joei.2022.06.004.

[8] C. Ma, Q. Yao, Y. Zhao, C. Zou, J. Zhao, Z. Miao, Gasification behavior and kinetics of chars derived from coal pyrolysis in a CO-containing atmosphere, J. Energy Inst. 109 (2023) 101299, https://doi.org/10.1016/j.joei.2023.101299.

[9] L. Ge, Y. Zhang, Z. Wang, J. Zhou, K. Cen, A novel power generation system based on the cascade utilization of coal: concept and preliminary experimental results, Energy Sources, Part A Recovery, Util. Environ. Eff. 39 (2017) 1955–1962, https://doi.org/10.1080/15567036.2013.828133.

[10] G. Zhang, Y. Yang, H. Jin, G. Xu, K. Zhang, Proposed combined-cycle power system based on oxygen-blown coal partial gasification, Appl. Energy 102 (2013) 735–745, https://doi.org/10.1016/j.apenergy.2012.08.019.

[11] Jing Zhou, Huang Zhong, R. Xiao, Air and steam coal partial gasification in an atmospheric fluidized bed, Energy Fuels 19 (2005) 1619–1623, https://doi.org/10.1021/ef0497558.

[12] C. Ye, Q. Wang, Y. Zheng, G. Li, Z. Zhang, Z. Luo, Techno-economic analysis of methanol and electricity poly-generation system based on coal partial gasification, Energy 185 (2019) 624–632, https://doi.org/10.1016/j.energy.2019.06.175.

[13] X. Song, Q. Wang, Y. Zhu, G. Xie, D. Zhu, J. Cen, Z. Luo, Experimental study on coal partial gasification coproducing char, tar, and gas, J. Therm. Sci. 32 (2023) 2297–2309, https://doi.org/10.1007/s11630-023-1832-9.

[14] C. Ye, Y. Zheng, Y. Xu, G. Li, C. Dong, Y. Tang, Q. Wang, Energy and exergy analysis of poly-generation system of hydrogen and electricity via coal partial gasification, Comput. Chem. Eng. 141 (2020) 106911, https://doi.org/10.1016/j.compchemeng.2020.106911.

[15] D.S. Upadhyay, A.K. Sakhiya, K. Panchal, A.H. Patel, R.N. Patel, Effect of equivalence ratio on the performance of the downdraft gasifier – an experimental and modelling approach, Energy 168 (2019) 833–846, https://doi.org/10.1016/j.energy.2018.11.133.

[16] D. Tokmurzin, D. Adair, T. Dyussekhanov, K. Suleymenov, B. Golman, B. Aiymbetov, Development of a circulating fluidized bed partial gasification process for co-production of metallurgical semi-coke and syngas and its integration with power plant for electricity production, International Journal of Coal Preparation and Utilization 42 (2022) 899–924, https://doi.org/10.1080/19392699.2019.1674842.

[17] S.P. Middleton, J.W. Patrick, A. Walker, The release of coal nitrogen and sulfur on pyrolysis and partial gasification in a fluidized bed, Fuel 76 (1997) 1195–1200, https://doi.org/10.1016/S0016-2361(97)00118-X.

[18] J. Zhang, W. Xie, X. Li, Q. Hao, H. Chen, X. Ma, In situ generation of nickel/carbon catalysts by partial gasification of coal char and application for methane decomposition, Int. J. Hydrogen Energy 44 (2019) 2633–2644, https://doi.org/10.1016/j.ijhydene.2018.12.005.

[19] J. Zhang, G. Zhang, M. Qi, H. Hu, X. Ma, Co-production of hydrogen-rich gas and porous carbon by partial gasification of coal char, Chem. Pap. 72 (2018) 273–287, https://doi.org/10.1007/s11696-017-0278-5.

[20] C. Ye, Q. Wang, Z. Luo, G. Xie, K. Jin, M. Siyil, K. Cen, Characteristics of coal partial gasification on a circulating fluidized bed reactor, Energy Fuels 31 (2017) 2557–2564, https://doi.org/10.1021/acs.energyfuels.6b02889.

[21] C. Ye, Q. Wang, L. Yu, Z. Luo, K. Cen, Characteristics of coal partial gasification experiments on a circulating fluidized bed reactor under CO2O2 atmosphere, Appl. Therm. Eng. 130 (2018) 814–821, https://doi.org/10.1016/j.applthermaleng.2017.11.071.

[22] Y. Huang, B. Jin, Z. Zhong, R. Xiao, H. Zhou, Effect of operating conditions on gas components in the partial coal gasification with air/steam, Kor. J. Chem. Eng. 24 (2007) 698–705, https://doi.org/10.1007/s11814-007-0029-3.

[23] M. Wang, G. Wei, S. Yang, R. Zhu, L. Yang, Effect of alkali (K/Na) metal vapor on the metallurgical properties of coke in CO2–O2–N2 mixed atmosphere, Energy 257 (2022) 124748, https://doi.org/10.1016/j.energy.2022.124748.

[24] Y. Zhang, J. Zhu, Q. Lyu, F. Pan, Experimental study on combustion characteristics of pulverized coal based on partial gasification of circulating fluidized bed, Energy Fuels 34 (2020) 989–995, https://doi.org/10.1021/acs.energyfuels.9b03733.

[25] M. Mayerhofer, P. Mitsakis, X. Meng, W. de Jong, H. Spliethoff, M. Gaderer, Influence of pressure, temperature and steam on tar and gas in allothermal fluidized bed gasification, Fuel 99 (2012) 204–209, https://doi.org/10.1016/j.fuel.2012.04.022.

[26] A. Gálvez-Pérez, M.A. Martín-Lara, M. Calero, A. Pérez, P. Canu, G. Blázquez, Experimental investigation on the air gasification of olive cake at low temperatures, Fuel Process. Technol. 213 (2021) 106703, https://doi.org/10.1016/j.fuproc.2020.106703.

[27] R. Xiao, B. Jin, H. Zhou, Y. Huang, M. Zhang, Effect of gasifying agent preheated temperature on partial gasification of coal in a pressurized spout-fluid bed, Proceedings of the CSEE 25 (2005) 109–113.

[28] Y. Bai, Y. Wang, S. Zhu, L. Yan, F. Li, K. Xie, Synergistic effect between CO2 and H2O on reactivity during coal chars gasification, Fuel 126 (2014) 1–7, https://doi.org/10.1016/j.fuel.2014.02.025.

[29] J. Xu, S. Su, Z. Sun, M. Qing, Z. Xiong, Y. Wang, L. Jiang, S. Hu, J. Xiang, Effects of steam and CO2 on the characteristics of chars during devolatilization in oxy-steam combustion process, Appl. Energy 182 (2016) 20–28, https://doi.org/10.1016/j.apenergy.2016.08.121.

[30] Z. Wang, L. Zhang, Y. Zhao, S. Feng, J. Ma, W. Kong, B. Shen, R. Sun, Experimental investigation on the evolution characteristics of anthracite-N and semi-coke reactivity under various O2/H2O pre-oxidation atmospheres, Fuel Process. Technol. 216 (2021) 106725, https://doi.org/10.1016/j.fuproc.2021.106725.

[31] O.O. Sonibare, T. Haeger, S.F. Foley, Structural characterization of Nigerian coals by X-ray diffraction, Raman and FTIR spectroscopy, Energy 35 (2010) 5347–5353, https://doi.org/10.1016/j.energy.2010.07.025.

[32] X. Li, J. Hayashi, C.-Z. Li, FT-Raman spectroscopic study of the evolution of char structure during the pyrolysis of a Victorian brown coal, Fuel 85 (2006) 1700–1707, https://doi.org/10.1016/j.fuel.2006.03.008.

[33] H.-L. Tay, S. Kajitani, S. Zhang, C.-Z. Li, Effects of gasifying agent on the evolution of char structure during the gasification of Victorian brown coal, Fuel 103 (2013) 22–28, https://doi.org/10.1016/j.fuel.2011.02.044.

[34] S. Zhang, J. Hayashi, C.-Z. Li, Volatilisation and catalytic effects of alkali and alkaline earth metallic species during the pyrolysis and gasification of Victorian brown coal. Part IX. Effects of volatile-char interactions on char–H2O and char–O2 reactivities, Fuel 90 (2011) 1655–1661.

[35] Y. Zhao, C. Xing, C. Shao, G. Chen, S. Sun, G. Chen, L. Zhang, J. Pei, P. Qiu, S. Guo, Impacts of intrinsic alkali and alkaline earth metals on chemical structure of low-rank coal char: semi-quantitative results based on FT-IR structure parameters, Fuel 278 (2020) 118229, https://doi.org/10.1016/j.fuel.2020.118229.

[36] L. Wu, J. Liu, J. Zhou, Q. Zhang, Y. Song, S. Du, W. Tian, Evaluation of tar from the microwave co-pyrolysis of low-rank coal and corncob using orthogonal-test-based grey relational analysis (GRA), J. Clean. Prod. 337 (2022) 130362, https://doi.org/10.1016/j.jclepro.2022.130362.

[37] L. Ge, Y. Zhang, Z. Wang, J. Zhou, K. Cen, Effects of microwave irradiation treatment on physicochemical characteristics of Chinese low-rank coals, Energy Convers. Manag. 71 (2013) 84–91, https://doi.org/10.1016/j.enconman.2013.03.021.

[38] H. Li, S. Shi, B. Lin, J. Lu, Q. Ye, Y. Lu, Z. Wang, Y. Hong, X. Zhu, Effects of microwave-assisted pyrolysis on the microstructure of bituminous coals, Energy 187 (2019) 115986, https://doi.org/10.1016/j.energy.2019.115986.

[39] D. Zhu, Q. Wang, G. Xie, Z. Ye, Z. Zhu, C. Ye, Effect of air equivalence ratio on the characteristics of biomass partial gasification for syngas and biochar co-production in the fluidized bed, Renew. Energy 222 (2024) 119881, https://doi.org/10.1016/j.renene.2023.119881.

[40] F. Emun, M. Gadalla, T. Majozi, D. Boer, Integrated gasification combined cycle (IGCC) process simulation and optimization, Comput. Chem. Eng. 34 (2010) 331–338, https://doi.org/10.1016/j.compchemeng.2009.04.007.

[41] L.A. Calderón, E. Chamorro, J.F. Espinal, Understanding the kinetics of carbon-hydrogen reaction: insights from reaction mechanisms on zigzag edges for homogeneous and heterogeneous formation of methane, Carbon 118 (2017) 597–606, https://doi.org/10.1016/j.carbon.2017.03.097.

[42] W.-C. Xu, A. Tomita, The effects of temperature and residence time on the secondary reactions of volatiles from coal pyrolysis, Fuel Process. Technol. 21 (1989) 25–37, https://doi.org/10.1016/0378-3820(89)90012-X.

[43] C. Liang, H. Zhang, Z. Zhu, Y. Na, Q. Lu, CO2-O2 gasification of a bituminous coal in circulating fluidized bed, Fuel 200 (2017) 81–88, https://doi.org/10.1016/j.fuel.2017.03.032.

[44] L. Wu, J. Liu, J. Zhou, Q. Zhang, Y. Song, S. Du, W. Tian, Evaluation of tar from the microwave co-pyrolysis of low-rank coal and corncob using orthogonal-test-based grey relational analysis (GRA), J. Clean. Prod. 337 (2022) 130362, https://doi.org/10.1016/j.jclepro.2022.130362.

[45] Y. Ban, L. Jin, K. Wang, Y. Li, H. Yang, H. Hu, Catalytic effect of industrial waste carbide slag on pyrolysis of low-rank coal, Energy 265 (2023) 126368, https://doi.org/10.1016/j.energy.2022.126368.

[46] F. Mao, J. Wang, H. Fan, Application of two-dimensional gas chromatography/time-of-flight mass spectrometry (GC × GC-TOFMS) for the thorough study of hydrocarbons in lignite pyrolysates, J. Anal. Appl. Pyrol. 157 (2021) 105178, https://doi.org/10.1016/j.jaap.2021.105178.

[47] H. Liu, L. Xu, D. Zhao, Q. Cao, J. Gao, S. Wu, Effects of alkali and alkaline-earth metals and retention time on the generation of tar during coal pyrolysis in a horizontal fixed-bed reactor, Fuel Process. Technol. 179 (2018) 399–406, https://doi.org/10.1016/j.fuproc.2018.07.032.

[48] M. Qing, S. Su, H. Chi, J. Xu, Z. Sun, J. Gao, K. Xu, S. Hu, Y. Wang, X. Hu, Relationships between structural features and reactivities of coal-chars prepared in CO2 and H2O atmospheres, Fuel 258 (2019) 116087, https://doi.org/10.1016/j.fuel.2019.116087.

[49] H.-L. Tay, S. Kajitani, S. Zhang, C.-Z. Li, Inhibiting and other effects of hydrogen during gasification: further insights from FT-Raman spectroscopy, Fuel 116 (2014) 1–6, https://doi.org/10.1016/j.fuel.2013.07.066.

[50] Y. Zhu, F. Tian, Y. Liu, L. Cui, Y. Dan, C. Du, D. Li, Comparison of the composition and structure for coal-derived and petroleum heavy subfraction by an improved separation method, Fuel 292 (2021) 120362, https://doi.org/10.1016/j.fuel.2021.120362.

[51] C. Zhao, L. Ge, L. Mai, S. Chen, Q. Li, L. Yao, D. Li, Y. Wang, C. Xu, Preparation and performance of coal-based activated carbon based on an orthogonal experimental study, Energy 274 (2023) 127353, https://doi.org/10.1016/j.energy.2023.127353.

[52] In situ FT-IR spectroscopic studies on thermal decomposition of the weak covalent bonds of brown coal, J. Anal. Appl. Pyrol. 115 (2015) 262–267, https://doi.org/10.1016/j.jaap.2015.08.002.

[53] V.I. Stenberg, M.B. Jones, N.J. Suwarnasarn, Radicals in coals during pyrolysis in relation to liquefaction conversion, Fuel 64 (1985) 470–474, https://doi.org/10.1016/0016-2361(85)90079-1.
[54] B. Wang, L. Sun, S. Su, J. Xiang, S. Hu, H. Fei, Char structural evolution during pyrolysis and its influence on combustion reactivity in air and oxy-fuel conditions, Energy Fuels 26 (2012) 1565–1574, https://doi.org/10.1021/ef201723q.
[55] K.S.W. Sing, Reporting physisorption data for gas/solid systems with special reference to the determination of surface area and porosity (Recommendations 1984), Pure Appl. Chem. 57 (1985) 603–619, https://doi.org/10.1351/pac198557040603.
[56] W.D. Machin, Temperature dependence of hysteresis and the pore size distributions of two mesoporous adsorbents, Langmuir 10 (1994) 1235–1240, https://doi.org/10.1021/la00016a042.